

# Impacts of Sea Ice Mushy Thermodynamics in the Antarctic on the Coupled Earth System

A. K. DuVivier<sup>1</sup>, M. M. Holland<sup>1</sup>, L. Landrum<sup>1</sup>, H. A. Singh<sup>2</sup>, D. A. Bailey<sup>1</sup>

<sup>1</sup>National Center for Atmospheric Research, Boulder, CO

<sup>2</sup>University of Victoria, Canada

## Key Points:

- Choice of sea ice thermodynamics does not lead to large differences in sea ice state due to compensating thermodynamic changes
- AABW production increases by 0.5 Sv and upper ocean becomes denser due to increasing salinity with mushy thermodynamics
- Wintertime air-sea fluxes, atmospheric low-level mixing, and low cloud cover all decrease with mushy thermodynamics

---

Corresponding author: A.K. DuVivier, [duvivier@ucar.edu](mailto:duvivier@ucar.edu)

## Abstract

We analyze two preindustrial experiments from the Community Earth System Model version 2 (CESM2) to characterize the impact of sea ice physics on regional differences in coastal sea ice production around Antarctica and the resulting impact on the ocean and atmosphere. The experiment in which sea ice is a “mushy” mixture of solid ice and brine has a substantial increase in coastal sea ice frazil and snow ice production that is accompanied by decreasing congelation growth and increasing bottom melt. With “mushy” ice physics, the subsurface ocean is denser and saltier, there is a statistically significant increase in Antarctic Bottom Water Formation by 0.5 Sv, but differences in ocean biogeochemistry are minimal and only in regions where the summer ice state differs. While there are no significant changes in the atmospheric circulation, using “mushy” ice physics results in decreased turbulent heat flux, atmospheric convection, and low level cloud cover.

## Plain Language Summary

We analyze experiments from the Community Earth System Model (CESM) to better understand the impacts of representing sea ice as a mixture of salty water and solid ice rather than just solid ice. We focus on sea ice produced around the Antarctic coasts and find that the ways in which the sea ice grow and melt change with the two representations of sea ice, but the differences compensate so that the average sea ice state is minimally changed. However, the near surface ocean water is denser in the experiment with sea ice represented by a mix of solid ice and salty water, mainly because the ocean is saltier. This leads to increased formation of dense Antarctic Bottom Water. In addition, there is less energy input into the atmosphere and less low level cloud cover around the Antarctic coasts in the experiment with the sea ice represented as a mix of salty water and solid ice. Thus, there are important impacts on the Earth system based solely on the way sea ice is represented.

## 1 Introduction

Cold, downslope winds continually push ice away from the Antarctic coast, creating coastal polynyas - areas of open ocean - where large quantities of frazil ice are formed (Massom et al., 1998; Morales Maqueda, 2004). There is elevated coastal sea ice production within polynyas (Tamura et al., 2016), and some estimates show that while coastal polynyas make up only 1% of the sea ice area, they produce 10% of the total Antarctic sea ice (Mohrmann et al., 2021). Indeed, satellite estimates along the Antarctic coast indicate

active ice production over 50% of the time during winter months (Nakata et al., 2021). In addition to being sea ice “factories”, polynyas are a source of heat and moisture to the atmosphere (Carrasco et al., 2003; Knuth & Cassano, 2014), a location of brine rejection necessary for formation of Antarctic Bottom Water (Fusco et al., 2009; Kern & Aliani, 2011), and impact Southern Ocean ecology at all levels from primary productivity to top predators (Arrigo & van Dijken, 2003; Karnovsky et al., 2007; Arrigo et al., 2015; Labrousse et al., 2019). Therefore, understanding polynyas and their impacts on the coupled earth system is important for a full understanding of the physical-biological Southern Ocean system.

Few analyses using coupled climate models have been conducted on coastal Antarctic polynyas to date. A recent analysis of state-of-the-art Earth system models indicates that the Community Earth System Model version 2 (CESM2) simulates reasonable coastal polynya area as compared to satellite observations (Mohrmann et al., 2021). There is also a significant increase in coastal frazil ice production for CESM2 as compared with a previous version of the model (Singh et al., 2020). The presence of frazil ice along coastal regions in Antarctic winter suggests the presence of open water from polynyas. However, the two versions of CESM have many structural differences, so the changes in ice growth processes could have multiple origins. Analysis of two CESM2 experiments that differ only with respect to the sea ice thermodynamics, shows that while sea ice thermodynamics have only a small impact on the hemispheric mean sea ice state, there are significant differences in hemispheric ice growth processes (Bailey et al., 2020).

Motivated by the importance of Antarctic coastal sea ice on the physical and biological systems, this study expands on Bailey et al. (2020) and Singh et al. (2020) by performing analysis of the coastal sea ice mass budget and driving processes in CESM2 over distinct Antarctic regions, as well as assessing the coupled impacts of changing sea ice processes on the ocean and atmosphere that have the potential for global impacts.

## 2 Data

The fully coupled preindustrial model experiments used in this study use CESM2, as described in detail by Danabasoglu et al. (2020), and CESM uses the CICE version 5 thermodynamic-dynamic sea ice model component (Hunke et al., 2015). Additionally, the CESM2 uses a salinity dependent freezing temperature (Assur, 1958), which results in lower freezing temperatures for ocean water with higher salinity and a higher melting

temperature for sea ice that has higher salinity. The experiments used in this study parallel those described by Bailey et al. (2020). We analyze two experiments that differ only with respect to the sea ice thermodynamics: the first uses a prescribed vertical salinity profile (Bitz & Lipscomb, 1999), which was standard in CESM1 (called BL99 hereafter), and the second uses a mushy-layer thermodynamics with prognostic salinity profile (Turner et al., 2013; Turner & Hunke, 2015), as is standard in CESM2. We will refer to these experiments as BL99 and MUSHY respectively.

To evaluate processes driving sea ice evolution we analyze the sea ice mass budget. It is important to note that the ocean model in CESM2 conserves ocean volume, so the ice-ocean exchanges use a virtual salt flux rather than true salt flux. The conversions to virtual salt flux require a reference salinity, and for consistency all ice-ocean fluxes use the same assumptions as those in the ocean model. While both the internal sea ice salinity and ocean salinity are prognostic and change in time, all fluxes between the ice and ocean assume that the ice has a salinity of  $4 \text{ g kg}^{-1}$  and the ocean has a salinity of  $34.8 \text{ g kg}^{-1}$ . Therefore, the model does not explicitly reject brine with a given salinity to the ocean, but changes in total ice volume growth will result in different freshwater exchange between the ice and ocean. Frazil production occurs when ocean water drops below the freezing point and predominantly occurs in regions where there is open ocean. Congelation ice production occurs when ice grows on the bottom of existing sea ice. Snow-ice formation occurs when snow on top of ice becomes submerged and freezes. We briefly describe the relevant difference in ice growth processes below, and further details about the MUSHY thermodynamics can be found in Turner and Hunke (2015). The mushy-layer thermodynamics account for gravity drainage of brine through the ice, melt water flushing, and salinity effects on snow-ice formation. Frazil ice is calculated by the ocean model, which passes the relevant heat flux to the sea ice model, which creates the correct ice volume for that heat flux. An important difference between MUSHY and BL99 is that in MUSHY the frazil ice that is formed is a combination of solid ice and brine while in BL99 the frazil ice is only solid ice. Thus, for the same latent heat release, the total ice volume calculated by MUSHY is higher than BL99 because of the combination of solid ice and brine, and the ice model passes corrective fluxes of freshwater and salt removal to the ocean model to ensure conservation of mass. Additionally, in BL99 when snow-ice forms the snow of thickness  $l$  and density of  $330 \text{ kg m}^{-3}$  is compacted to form solid ice of thickness  $0.36l$  with density of  $917 \text{ kg m}^{-3}$ . In contrast, in MUSHY when snow-ice forms, the snow of thickness  $l$  is flooded by ocean water with the sea surface salinity to

form ice with thickness  $l$  with a porosity of 0.36. In both cases, given the same conditions a larger volume of ice is formed with MUSHY than BL99, which will result in more freshwater and salt removal from the ocean.

Both experiments branch off the CMIP6 preindustrial control at year 871 and run for 100 additional years. We use monthly mean output from all 100 years in order to account for substantial internal variability in the Antarctic sea ice state (Landrum et al., 2012). We performed the analysis over the first and last 50 year periods but the conclusions are the same as those over all 100 years, so we keep the full 100 year period for increased statistical robustness. These experiments have nominal  $1^\circ$  resolution, which is relevant for the fidelity of the model's representation of coastal areas.

In order to better understand possible differences in regional response, we have divided the Antarctic into five regional sectors shown on Figure 1 -Weddell Sea (Wed), Indian Ocean (Ind), Pacific Ocean (Pac), Ross Sea (Ross), and Amundsen-Bellinghshausen Sea (AB). Additionally, we primarily focus on the coastal regions (see 1a,b,c) and mask out the other areas with sea ice because on average 56% of the total sea ice produced over the Antarctic during the winter growth season (April-Sept), for both MUSHY and BL99 is formed in these coastal grid cells and thus they are important sea ice factories for the Antarctic.

### 3 Results

#### 3.1 Coastal Sea Ice Differences

Consistent with Bailey et al. (2020), we find that year-round differences in sea ice area and volume between the MUSHY and BL99 runs are small along the coast but that MUSHY has slightly higher ice concentrations and ice thicknesses (Figures S1, S2, S3). The largest differences are in the Amundsen-Bellinghshausen Sea where there is more extensive and thicker sea ice along the coast in the MUSHY experiment.

In contrast to the small ice state differences, there are significant differences in sea ice growth between the MUSHY and BL99 experiments, particularly over coastal regions (Figures 1 and S4). In winter, coastal congelation ice growth decreases in all sectors (Figures 1a and S5) while there are increases in both frazil and snow-ice formation (Figure 1b,c). In MUSHY there are also significant increases in winter ice mass loss due to bottom melt in all sectors and dynamic advection out of the coastal areas, primarily in the Indian Ocean and Pacific Ocean sectors (Figure S5).

The differences in coastal processes compensate such that the result is a similar mean sea ice state in MUSHY and BL99. When we examine thermodynamics processes alone we find that there is a significant increase in winter ice growth due to the large increase in frazil and snow-ice growth in MUSHY, but in opposition to these processes are decreases in congelation growth and increases in bottom melt (Figure 1e). This increase in net ice growth throughout the winter due to thermodynamics is relevant to the freshwater fluxes with the ocean. The increase in thermodynamics growth is compensated by increased dynamical ice loss such that the net coastal mass budget is only significantly different in the early freeze up period (Figure 1e), which can explain the slightly higher ice concentrations and thicknesses in MUSHY (Figure S1).

### 3.2 Impacts on the Ocean

There are significant differences in the mean ocean response to the difference in sea ice thermodynamics and dominant ice growth processes. The MUSHY experiment has greater winter potential density (as shown by change in sigma) and salinity originating at the surface along the coast and propagating downward (Figures 2d,e, S6, S7). In contrast, the differences in winter temperature are small and generally statistically insignificant near the surface and coast, but there tends to be warming below the mixed layer (Figures 2f, S8). The increases in density and salinity are consistent in all sectors at depth (Figure 2g,h). These increases in density are primarily related to the increase in salinity as the ocean temperature is either slightly warmer, which would act to lower density, in MUSHY or statistically insignificantly different.

The differences in ocean density impact the meridional overturning circulation (MOC) and Antarctic Bottom Water (AABW) formation. The maximum of sinking water in the MOC occurs at the same latitude (69°S) in both experiments (Figure 3a). However, the MOC difference indicates that in MUSHY the MOC has slightly weakened at sigma values of 36.5-37.0 kg m<sup>-3</sup> at more southern latitudes, but at sigma values of 37.0-37.5 kg m<sup>-3</sup> the MOC strengthens. The 100 year time series of AABW formation in both experiments shows that for MUSHY there is a statistically significant increase in annual mean AABW production by about 0.5 Sv (Figure 3c).

The impact of the differences in wintertime sea ice growth processes does not have a significant impact on summertime ocean chlorophyll levels. While the highest summertime

chlorophyll levels occur in regions co-located with wintertime polynyas, the difference in chlorophyll over the top 100 m is insignificant between MUSHY and BL99 in most locations (Figure S9). At only two locations are chlorophyll levels significantly different and those are areas where the summertime ice state is significantly different (Figure S1). First, in the AB sector there is a decrease in chlorophyll that is co-located with significantly higher summertime sea ice concentration and thickness for MUSHY, and second, in the Ind sector there are significant increases in chlorophyll along the coast where the sea ice concentration and thickness are significantly lower in MUSHY.

### 3.3 Impacts on the Atmosphere

The impact of sea ice thermodynamics on the ocean are confined to the coastal areas and lower atmosphere. Along the Antarctic coasts, where there is slightly higher ice concentration and thickness in MUSHY (Figure S1), in MUSHY there are generally weaker turbulent heat fluxes (Figure 4a). The average decrease in turbulent heat flux is  $-3 \text{ W m}^2$  (-7% change), though the decrease in average fluxes in the Indian Ocean and Pacific Ocean sectors are  $-5.5$  and  $-6.7 \text{ W m}^2$  (-11% change) respectively. The change in turbulent flux is driven primarily by changes in the sensible heat flux (Figure S10). This decrease in energy fluxed into the atmosphere leads to small but significant decreases in atmospheric planetary boundary height and low cloud cover near the Antarctic coasts (Figure 4b,c). Yet, there are not significant changes in wintertime sea level pressure (Figure S11a) or 500 hPa geopotential heights (not shown). Additionally, there are no significant differences along the coasts in near-surface temperature or moisture (Figure S11b,c). The significant differences in coastal precipitation and wind speed vary in sign and magnitude in different Antarctic sectors (Figure S11d,e), which suggests there is not a consistent impact of sea ice thermodynamics on these fields. Thus, while the MUSHY thermodynamics leads to local changes in atmospheric mixing and heat fluxes along the coast, on the whole it does not strongly impact the atmospheric circulation or drive consistent changes in precipitation.

## 4 Discussion and Conclusions

This paper addresses questions about the impact of sea ice thermodynamics on the coupled Earth System. We find that while changing the sea ice thermodynamics does not have a large impact on the sea ice mean state, there are significant changes in both the processes that drive sea ice evolution and the coupled impacts on the ocean and atmosphere.

With the MUSHY thermodynamics, along the Antarctic coasts and in all sectors a statistically significant increase in frazil and snow-ice growth is partly compensated by decreases in congelation ice growth and increase in bottom melt throughout the ice growth season. Increases in frazil ice are caused in part by the larger volume of ice created in MUSHY due to the combination of solid ice and brine as well as increased dynamic loss in some sectors that would cause more open water. The increase in snow-ice formation is not related to changes in precipitation, which are insignificant and differ in sign across coastal locations. Instead, the increase in snow-ice growth is due in part because there is a larger volume of ice from flooding rather than compacting snow, and partly from the increase in bottom melt that would thin the ice and make it easier for snow to go below sea level. The increase in sea ice bottom melt is likely related to the combination of a salinity dependent freezing point and the prognostic internal ice salinity. In MUSHY the bulk ice salinity is saltier than in BL99 (Turner & Hunke, 2015). Saltier ice has a lower freeze-melt point, leading to decreased congelation growth and increased bottom melt at lower temperatures.

The changes in the sea ice processes have a significant impact on the ocean state and MOC. Due to the larger volume of ice formed in MUSHY, there is more freshwater removal and the ocean becomes saltier and denser from the surface. In contrast, there are minimal changes in the ocean temperature, particularly near the surface. Thus, the changes in salinity are primarily driving the changing density. The MOC strengthens for higher ocean water densities and there is a small, but significant, increase in AABW formation in the MUSHY experiment. Because AABW is the densest water mass in the global oceans and an important component of the global thermohaline circulation, changes in this water mass due to sea ice thermodynamics have the potential for possible global impacts. Differences in coastal chlorophyll production are highly correlated with areas that have differences in summer sea ice state rather than changes in the ocean state.

In contrast to the relatively widespread impacts on the ocean from changing sea ice physics, the atmospheric impacts are mostly confined to the Antarctic coastal regions. The declines in coastal turbulent heat fluxes to the atmosphere with the MUSHY mean less energy is entering the atmosphere during wintertime. This leads to shallower atmospheric boundary layer depths and therefore less atmospheric mixing as well as decreases in low-level cloud cover. Yet these coupled atmospheric effects are local and do not appear to impact the large scale atmospheric circulation or state. There are not significant or consistent changes to atmospheric circulation, near surface winds, temperature, or humidity. While

the majority of this study focuses on coastal impacts of sea ice thermodynamics, there are significant off-coast atmospheric impacts in the vicinity of the Amundsen Sea Low (Raphael et al., 2016) from sea ice thermodynamics. In this area there are increased turbulent heat fluxes and planetary boundary layer heights (Figure 4a,b) as well as increased 2m Temperature and humidity (Figure S11b,c). It is also important to note that these differences in atmospheric response occur along the winter ice edge where there are significant decreases in ice concentration and thickness in the MUSHY experiment (Figure S1a,b). We found that the decrease in ice concentration is due to thermodynamic processes, in particular the decreases in congelation and frazil ice growth and increases in bottom melt in the MUSHY experiment as compared with the BL99 (not shown).

A number of questions and limitations remain. First, CESM2 simulations are relatively coarse in resolution. The CESM2 experiments are nominally  $1^\circ$  resolution, which results in sea ice and ocean grid 40-60km grid boxes near the Antarctic coasts. Yet, coastal polynyas occur on small spatial scales that may require much higher resolution to fully capture and would therefore be missed in these CESM2 experiments. Additionally, while CESM2 uses a state-of-the-science sea ice model, CICE5, there may still be missing coastal processes that are important for forming polynyas. For example, ice tongues, fast-ice that is fixed to the ocean bottom, or pancake ice formation are not included as physical processes represented by CICE5 in the CESM2, yet observations have shown these impact polynya formation (Tison et al., 2020; Thompson et al., 2020). Moreover, because the CESM2 ocean model requires a virtual salt flux exchange the prognostic ice salinity is not directly coupled with the ocean salinity and there is not explicit salt injection into the ocean. We are actively working in implementing a true salt flux coupling in CESM that will alleviate some of these concerns. Finally, we have used coastal ice production as a metric to imply the existence of polynyas. However, we find that the monthly mean ice concentration through winter season is nearly 100% along the entire coast. We believe this may be the result of using monthly data rather than daily data, which may be able to better identify short-lived polynya events but further analysis is needed with higher temporal frequency data to understand the shorter timescale of polynya events. An outstanding question is to better understand the optimal way to define a polynya, especially within a model where it is possible to have 100% ice concentration of thin ice that a satellite might still detect as open ocean and what the best methods are to compare with observations.

## Acknowledgments

The CESM project is supported primarily by the National Science Foundation (NSF). This material is based upon work supported by the National Center for Atmospheric Research (NCAR), which is a major facility sponsored by the NSF under Cooperative Agreement 1852977. Computing and data storage resources, including the Cheyenne supercomputer (doi:10.5065/D6RX99HX), were provided by the Computational and Information Systems Laboratory (CISL) at NCAR. We thank all the scientists, software engineers, and administrators who contributed to the development of CESM2. MMH and LL acknowledge support from NASA grant 80NSSC20K1289.

Previous and current CESM versions are freely available online (at <https://www.cesm.ucar.edu/models/cesm2/>). The CESM data sets used in this study will be made available upon acceptance of the manuscript from the Earth System Grid Federation (ESGF) at <https://esgf-node.llnl.gov/Fsearch/cmip6>, or from the NCAR Digital Asset Services Hub (DASH) at <https://data.ucar.edu>, or from the links provided from the CESM website (at <https://www.cesm.ucar.edu>).

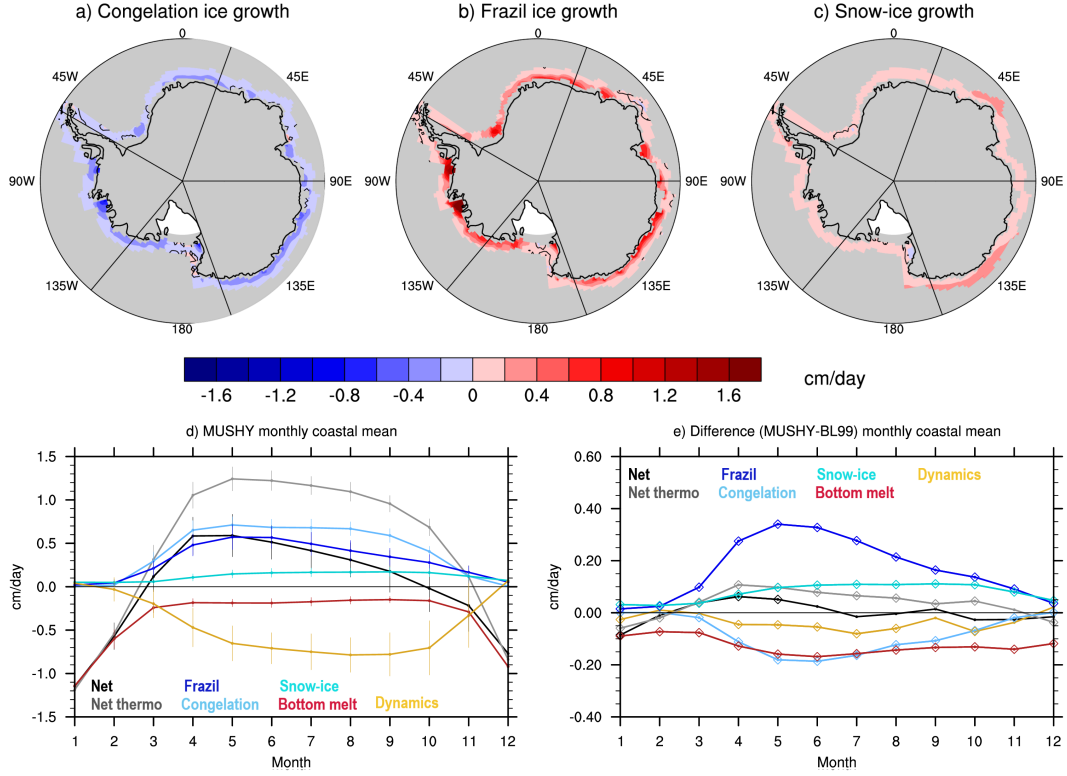
## References

- Arrigo, K. R., & van Dijken, G. L. (2003). Phytoplankton dynamics within 37 Antarctic coastal polynya systems. *Journal of Geophysical Research*, *108*(C8). doi: 10.1029/2002JC001739
- Arrigo, K. R., van Dijken, G. L., & Strong, A. L. (2015, August). Environmental controls of marine productivity hot spots around Antarctica. *Journal of Geophysical Research: Oceans*, *120*(8), 5545–5565. doi: 10.1002/2015JC010888
- Assur, A. (1958). Arctic sea ice. *National Academy of Sciences-National Research Council. Chap. Composition of sea ice and its tensile strength*, 106–138.
- Bailey, D. A., Holland, M. M., DuVivier, A. K., Hunke, E. C., & Turner, A. K. (2020). Impact of Sea Ice Thermodynamics in the CESM2 sea ice component. *Journal of Advances in Modeling Earth Systems*. doi: 10.1029/2020MS002154
- Bitz, C. M., & Lipscomb, W. H. (1999). An energy-conserving thermodynamic model of sea ice. *Journal of Geophysical Research: Ocean*, *104*(C7), 15669–15677. doi: 10.1029/1999JC900100
- Carrasco, J. F., Bromwich, D. H., & Monaghan, A. J. (2003). Distribution and Characteristics of Mesoscale Cyclones in the Antarctic: Ross Sea Eastward to the Weddell Sea. *MONTHLY WEATHER REVIEW*, *131*, 289–301. doi: 10.1175/1520-0493(2003)

- 131 10.1029/2019MS001916
- 298 131 10.1029/2019MS001916
- 299 Danabasoglu, G., Lamarque, J., Bacmeister, J., Bailey, D. A., DuVivier, A. K., Edwards,  
 300 J., ... Strand, W. G. (2020, February). The Community Earth System Model Version  
 301 2 (CESM2). *Journal of Advances in Modeling Earth Systems*, 12(2), e2019MS001916.  
 302 doi: 10.1029/2019MS001916
- 303 Fusco, G., Budillon, G., & Spezie, G. (2009, August). Surface heat fluxes and thermohaline  
 304 variability in the Ross Sea and in Terra Nova Bay polynya. *Continental Shelf Research*,  
 305 29(15), 1887–1895. doi: 10.1016/j.csr.2009.07.006
- 306 Hunke, E. C., Lipscomb, W. H., Turner, A. K., Jeffery, N., & Elliott, S. (2015). *CICE:  
 307 the Los Alamos Sea Ice Model Documentation and Software User's Manual Version 5.*  
 308 (Tech. Rep.). Los Alamos, NM: Los Alamos National Laboratory.
- 309 Karnovsky, N., Ainley, D., & Lee, P. (2007). Chapter 12 The Impact and Importance of  
 310 Production in Polynyas to Top-Trophic Predators: Three Case Histories. In *Elsevier  
 311 Oceanography Series* (Vol. 74, pp. 391–410). Elsevier. doi: 10.1016/S0422-9894(06)  
 312 74012-0
- 313 Kern, S., & Aliani, S. (2011). A comparison between polynya area and associated ice  
 314 production with mooring-based measurements of temperature, salinity and currents  
 315 in the southwestern Ross Sea, Antarctica. *Annals of Glaciology*, 52(57), 291–300.
- 316 Knuth, S. L., & Cassano, J. J. (2014, September). Estimating Sensible and Latent Heat  
 317 Fluxes Using the Integral Method from in situ Aircraft Measurements. *Journal of  
 318 Atmospheric and Oceanic Technology*, 31(9), 1964–1981. doi: 10.1175/JTECH-D-14  
 319 -00008.1
- 320 Labrousse, S., Fraser, A. D., Sumner, M., Tamura, T., Pinaud, D., Wienecke, B., ... Jenou-  
 321 vrier, S. (2019, October). Dynamic Fine-Scale Sea Icescape Shapes Adult Emperor  
 322 Penguin Foraging Habitat in East Antarctica. *Geophysical Research Letters*, 46(20),  
 323 11206–11218. doi: 10.1029/2019GL084347
- 324 Landrum, L., Holland, M. M., Schneider, D. P., & Hunke, E. (2012). Antarctic sea ice  
 325 climatology, variability, and late twentieth-century change in cesm4. *Journal of Cli-  
 326 mate*, 25(14), 4817 - 4838. Retrieved from [https://journals.ametsoc.org/view/  
 327 journals/clim/25/14/jcli-d-11-00289.1.xml](https://journals.ametsoc.org/view/journals/clim/25/14/jcli-d-11-00289.1.xml) doi: 10.1175/JCLI-D-11-00289.1
- 328 Massom, R. A., Harris, P., Michael, K. J., & Potter, M. (1998). The distribution and  
 329 formative processes of latent-heat polynyas in East Antarctica. *Annals of Glaciology*,  
 330 27, 420–426. doi: 10.3189/1998AoG27-1-420-426

- 331 Mohrmann, M., Heuzé, C., & Swart, S. (2021). Southern Ocean polynyas in CMIP6 models.  
332 *The Cryosphere Discussions*, 2021, 1–43. doi: 10.5194/tc-2021-23
- 333 Morales Maqueda, M. A. (2004). Polynya Dynamics: a Review of Observations and Mod-  
334 eling. *Reviews of Geophysics*, 42(1). doi: 10.1029/2002RG000116
- 335 Nakata, K., Ohshima, K. I., & Nihashi, S. (2021). Mapping of Active Frazil for Antarctic  
336 Coastal Polynyas, With an Estimation of Sea-Ice Production. *Geophysical Research*  
337 *Letters*, 11. doi: 10.1029/2020GL091353
- 338 Raphael, M. N., Marshall, G. J., Turner, J., Fogt, R. L., Schneider, D., Dixon, D. A., ...  
339 Hobbs, W. R. (2016). The Amundsen Sea Low: Variability, Change, and Impact on  
340 Antarctic Climate. *Bulletin of the American Meteorological Society*, 97(1), 111–121.  
341 doi: 10.1175/BAMS-D-14-00018.1
- 342 Singh, H. K. A., Landrum, L., Holland, M. M., Bailey, D., & DuVivier, A. (2020). An  
343 Overview of Antarctic Sea Ice in the CESM2: Analysis of the Seasonal Cycle, Pre-  
344 dictability, and Atmosphere-Ocean-Ice Interactions. *Journal of Advances in Modeling*  
345 *Earth Systems*. doi: 10.1029/2020MS002143
- 346 Tamura, T., Ohshima, K. I., Fraser, A. D., & Williams, G. D. (2016, May). Sea ice  
347 production variability in Antarctic coastal polynyas. *Journal of Geophysical Research:*  
348 *Oceans*, 121(5), 2967–2979. doi: 10.1002/2015JC011537
- 349 Thompson, L., Smith, M., Thomson, J., Stammerjohn, S., Ackley, S., & Loose, B. (2020).  
350 Frazil ice growth and production during katabatic wind events in the Ross Sea, Antarc-  
351 tica. *The Cryosphere*, 14(10), 3329–3347. doi: 10.5194/tc-14-3329-2020
- 352 Tison, J.-L., Maksym, T., Fraser, A. D., Corkill, M., Kimura, N., Nosaka, Y., ... Delille,  
353 B. (2020, June). Physical and biological properties of early winter Antarctic sea ice  
354 in the Ross Sea. *Annals of Glaciology*, 1–19. doi: 10.1017/aog.2020.43
- 355 Turner, A. K., & Hunke, E. C. (2015, February). Impacts of a mushy-layer thermody-  
356 namic approach in global sea-ice simulations using the CICE sea-ice model. *Journal*  
357 *of Geophysical Research: Oceans*, 120(2), 1253–1275. doi: 10.1002/2014JC010358
- 358 Turner, A. K., Hunke, E. C., & Bitz, C. M. (2013, May). Two modes of sea-ice grav-  
359 ity drainage: A parameterization for large-scale modeling. *Journal of Geophysical*  
360 *Research: Oceans*, 118(5), 2279–2294. doi: 10.1002/jgrc.20171

361

**Figures**

**Figure 1.** Winter (April-Sept) mean difference of a) congelation growth, b) frazil growth, and c) snow-ice growth; regions that are significantly different at the 95% confidence level do not have stippling. d) MUSHY mean and e) difference in monthly coastal mean mass budget terms - Net ice growth/melt (black), net thermodynamic ice growth/melt (gray), frazil growth (dark blue), congelation growth (light blue), snow-ice growth (teal), bottom melt (red), and dynamics (gold). Mean budget terms include two standard deviations and differences significant at the 95% confidence level have a diamond marker. All differences show MUSHY minus BL99 and units are  $\text{cm day}^{-1}$ .

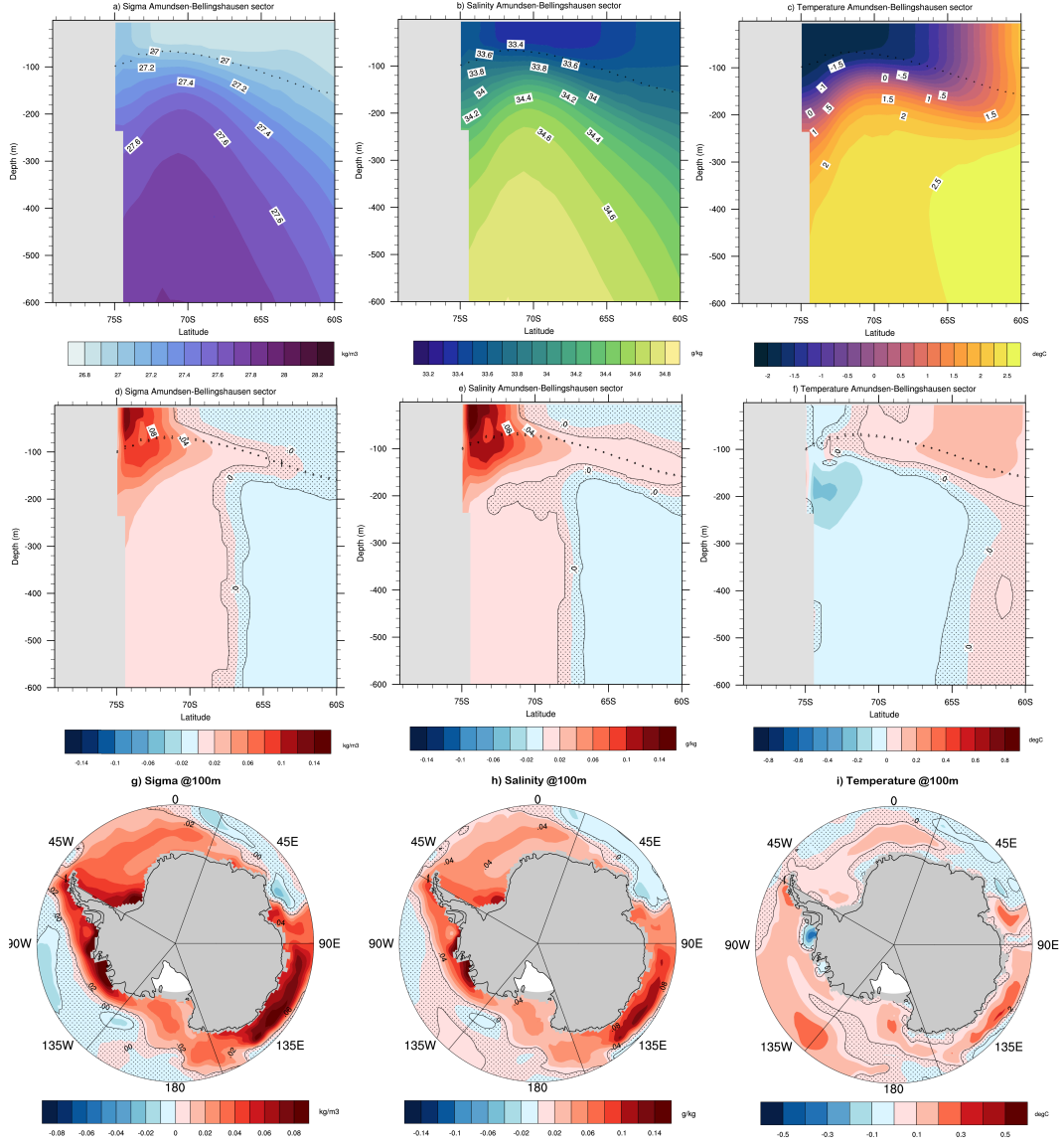


**Figure 2.** Winter (April-Sept) (a,b,c) mean and (d,e,f) transects averaged over the Amundsen-Bellinghousen sector, and (g,h,i) differences at 100m depth for sigma (a,d,g; kg m<sup>-3</sup>), salinity (b,e,h; g kg<sup>-1</sup>), and temperature (c,f,i; °C). All differences show MUSHY minus BL99 and regions that are significantly different at the 95% confidence level do not have stippling. For the transects, the MUSHY mixed layer depth is shown by plus symbols and the BL99 mixed layer depth is shown by open circles.

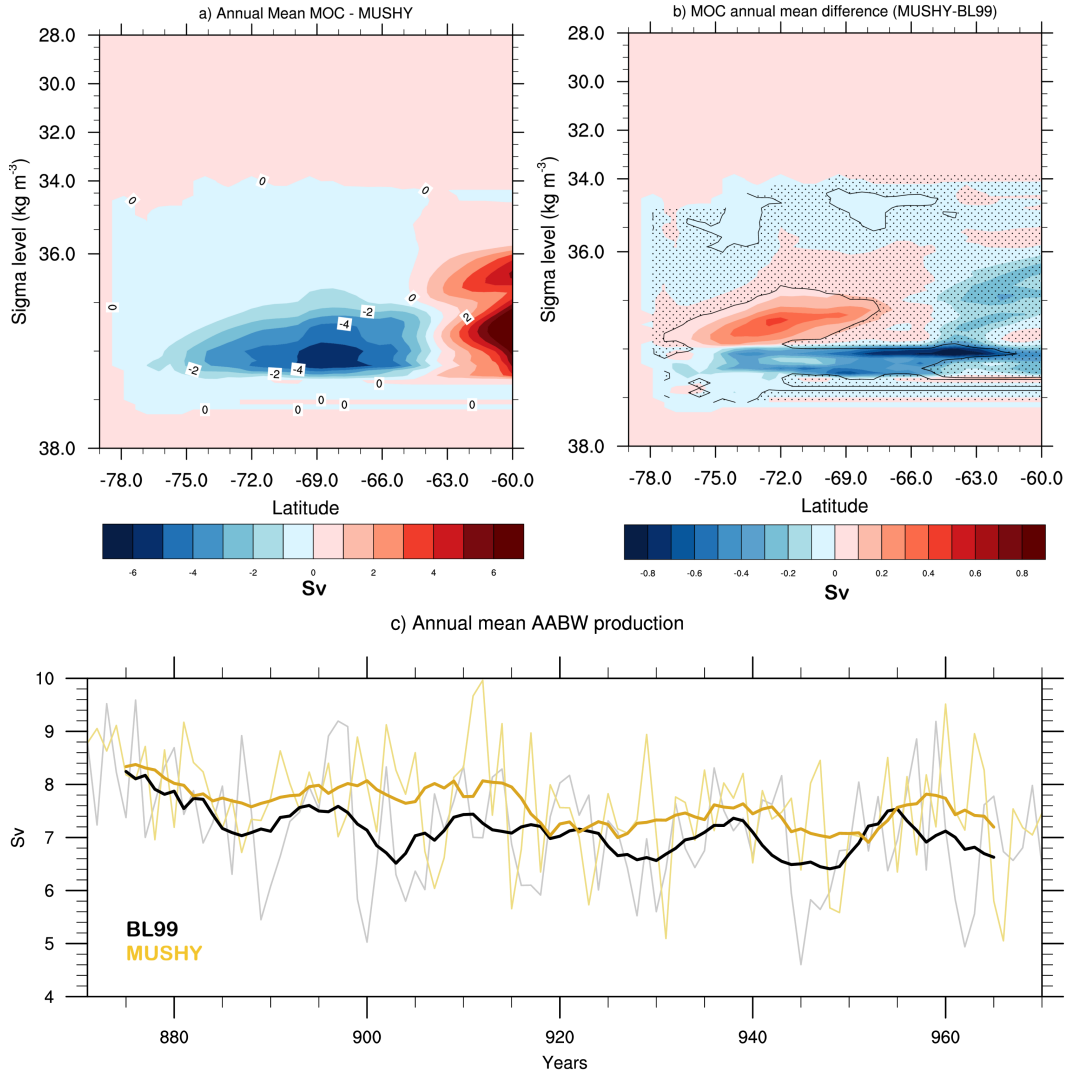


**Figure 3.** Annual mean of meridional overturning circulation (MOC;  $\text{Sv}$ ) mapped to isopycnals for a) MUSHY and b) difference (MUSHY minus BL99) where values that are significantly different at the 95% confidence level do not have stippling. c) 10 year running mean and annual mean values time series of the BL99 (black) and MUSHY (gold) annual mean Antarctic Bottom Water (AABW) formation ( $\text{Sv}$ ) where the running mean is shown by the bold line.

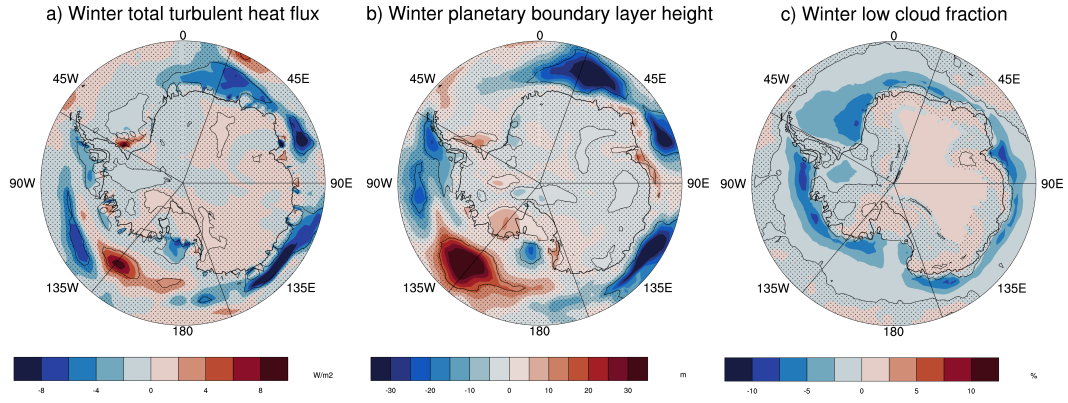


**Figure 4.** Winter (Apr-Sept) mean difference of a) total turbulent heat flux ( $\text{W m}^{-2}$ ), b) atmospheric boundary layer height (m), and c) winter cloud fraction (%). All differences show MUSHY minus BL99 and regions that are significantly different at the 95% confidence level do not have stippling.

362  
363

Supporting Information - copied to SI file, but here for now so that references in Latex work properly

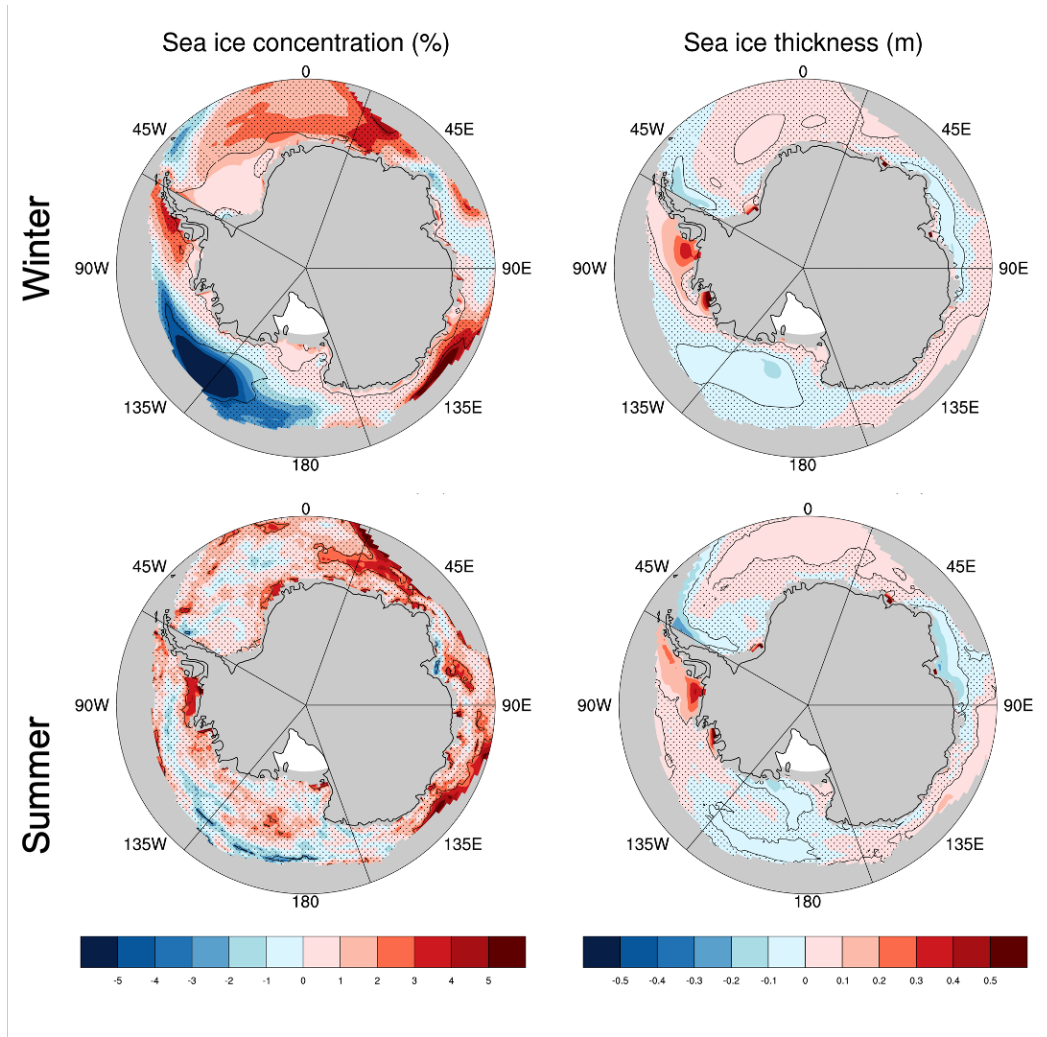


**Figure S1.** Winter (April-Sept; top row) and Summer (Oct-Mar; bottom row) mean difference (MUSHY-BL99) of sea ice concentration (left column; %) and sea ice thickness (right column; m). Points that are significantly different at the 95% confidence level do not have stippling.

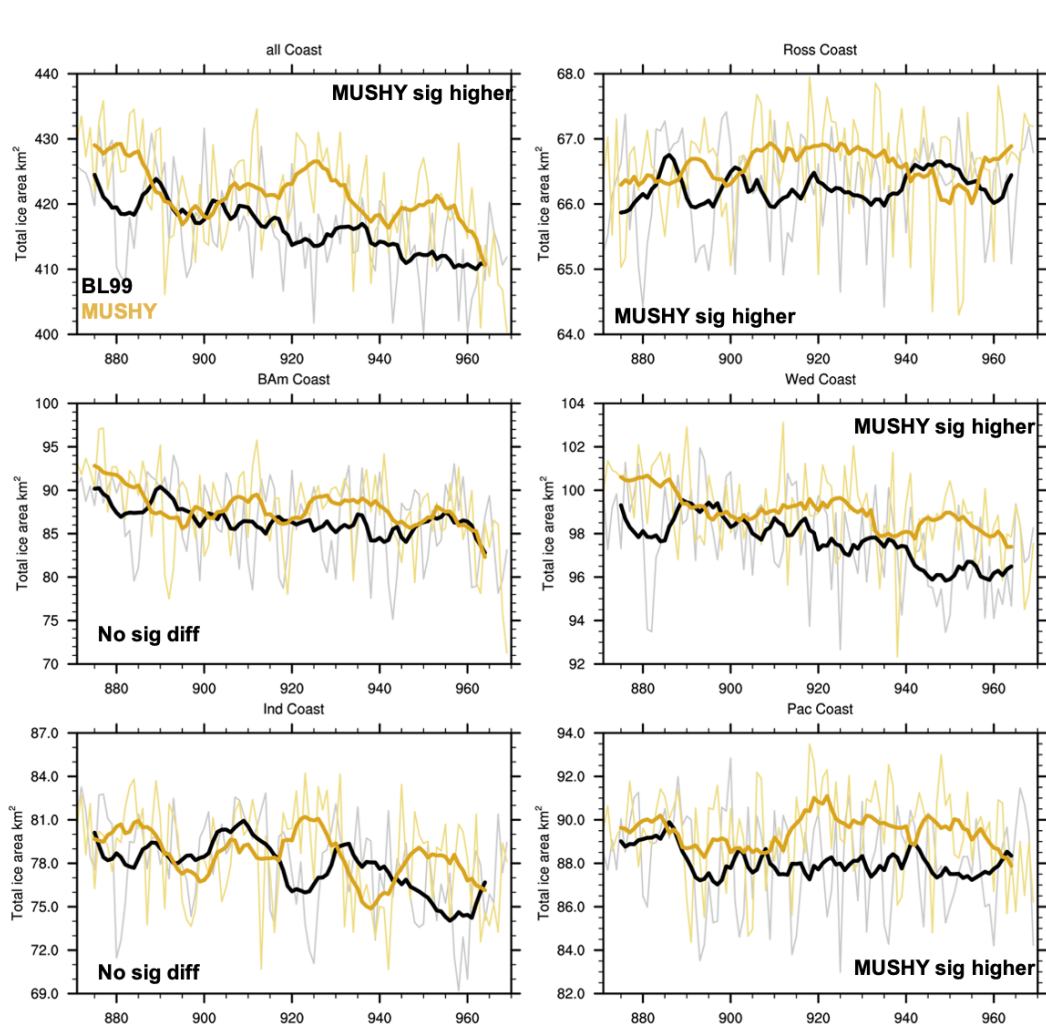


**Figure S2.** Winter (April-Sept) time series of BL99 (black) and MUSHY (gold) total ice area (km<sup>2</sup>) along coastal points for a) all coasts, b) Ross sector, c) Amundsen-Bellingshausen sector, d) Weddell sector, e) Indian Ocean sector, and f) Pacific Ocean sector.

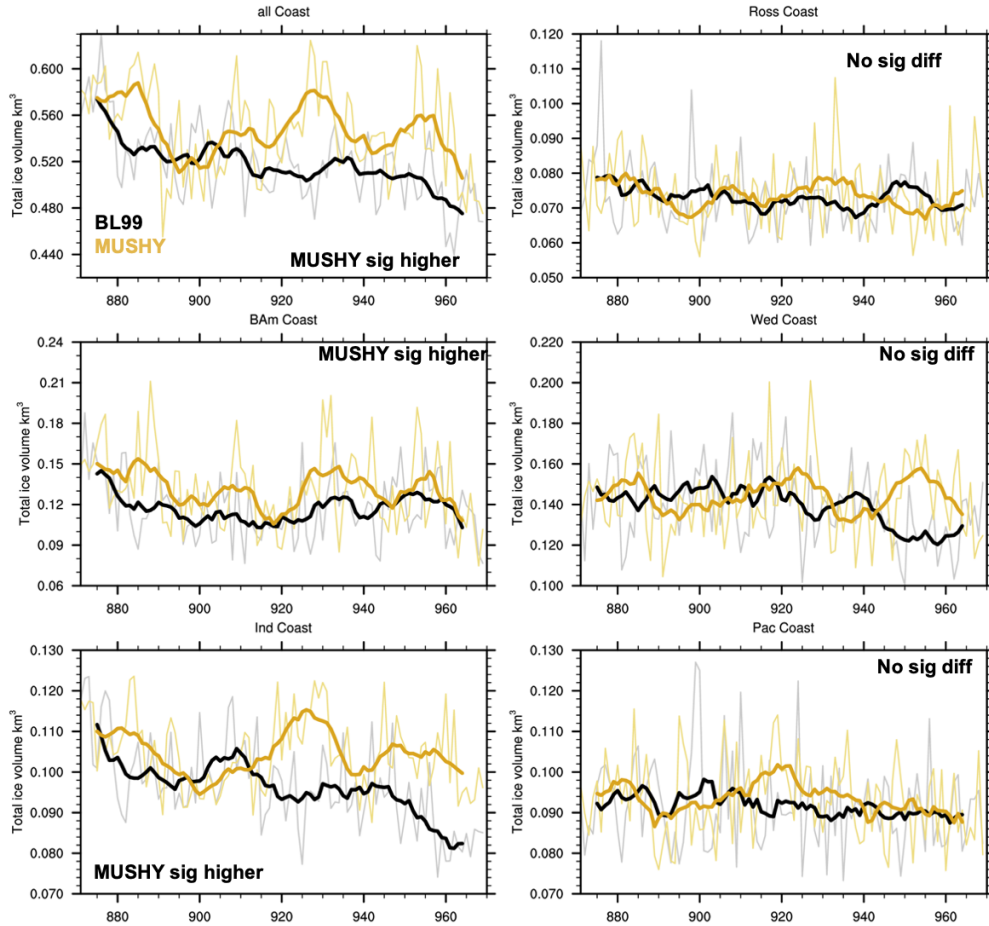


**Figure S3.** Winter (April-Sept) time series of BL99 thermo (black) and MUSHY (gold) total ice volume (km<sup>3</sup>) along coastal points for a) all coasts, b) Ross sector, c) Amundsen-Bellingshausen sector, d) Weddell sector, e) Indian Ocean sector, and f) Pacific Ocean sector.

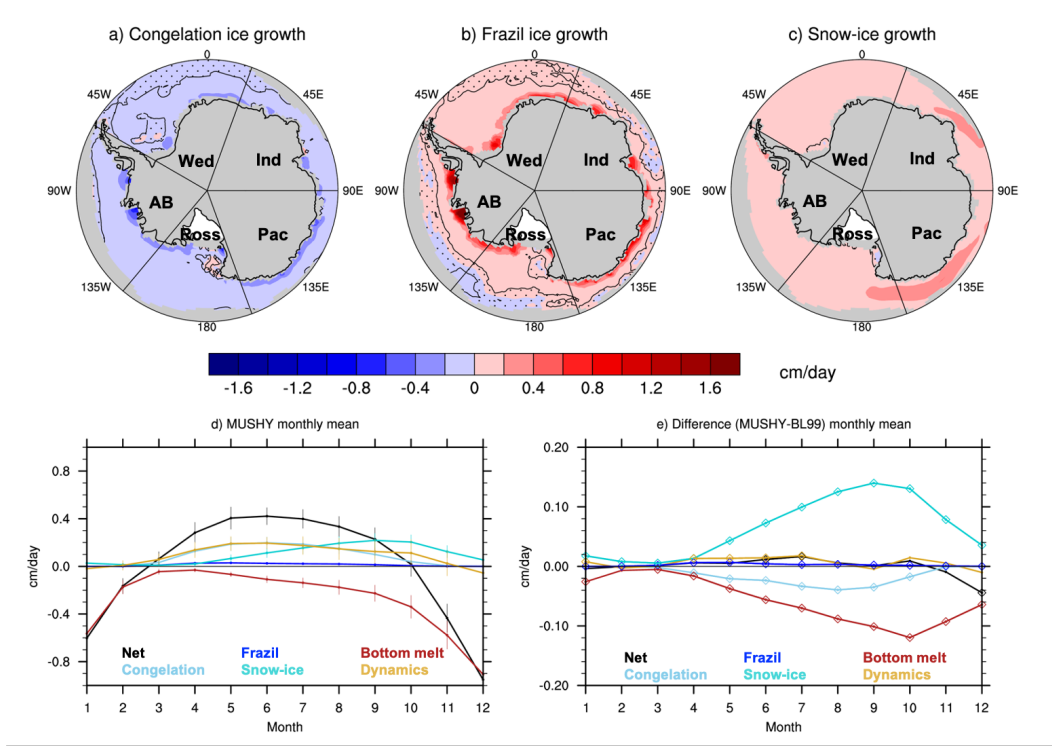


**Figure S4.** Winter (April-Sept) mean difference of a) congelation growth, b) frazil growth, and c) snow-ice growth; regions that are significantly different at the 95% confidence level do not have stippling. Monthly mean mass budget terms - Net ice growth/melt (black), net thermodynamic growth/melt (grey), frazil growth (dark blue), congelation growth (light blue), snow-ice growth (teal), bottom melt (red), and dynamics (gold) - for d) MUSHY and e) differences ( $\text{cm day}^{-1}$ ). Vertical lines on the mean budget terms indicate two standard deviations and differences significant at the 95% confidence level have a diamond marker. All differences show MUSHY-BL99.

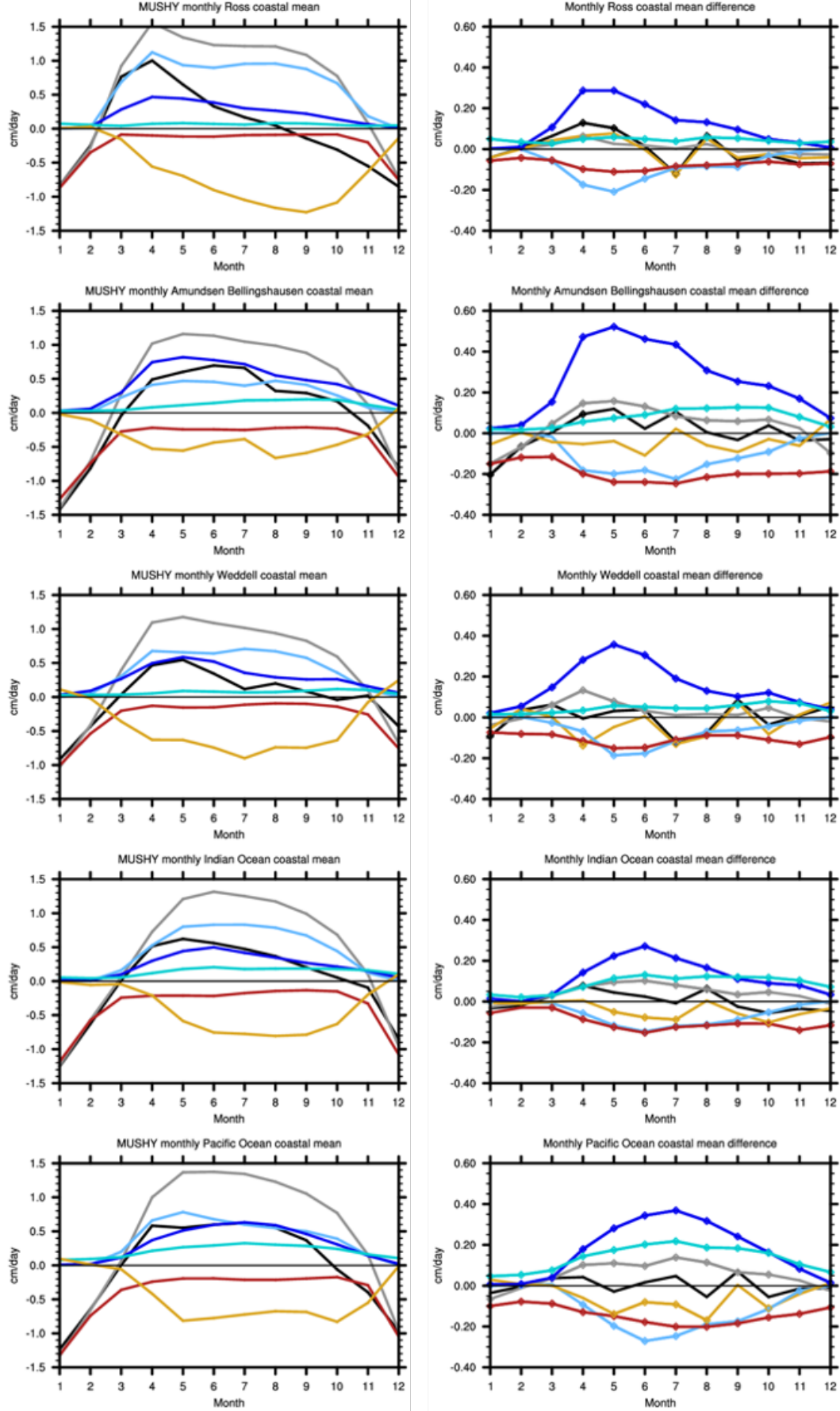


**Figure S5.** Monthly coastal mean mass budget terms (cm day<sup>-1</sup>) for MUSHY (left column) and difference (MUSHY-BL99, right column): net ice mass budget (black), net thermodynamic growth/melt (grey); congelation growth (light blue), frazil growth (dark blue), snow-ice growth (teal), bottom melt (red), and dynamics (gold) for the: Ross Sea sector (top row), Amundsen-Bellinghousen sector (second row), Weddell sector (third row), Indian Ocean sector (fourth row), Pacific Ocean sector (fifth row).

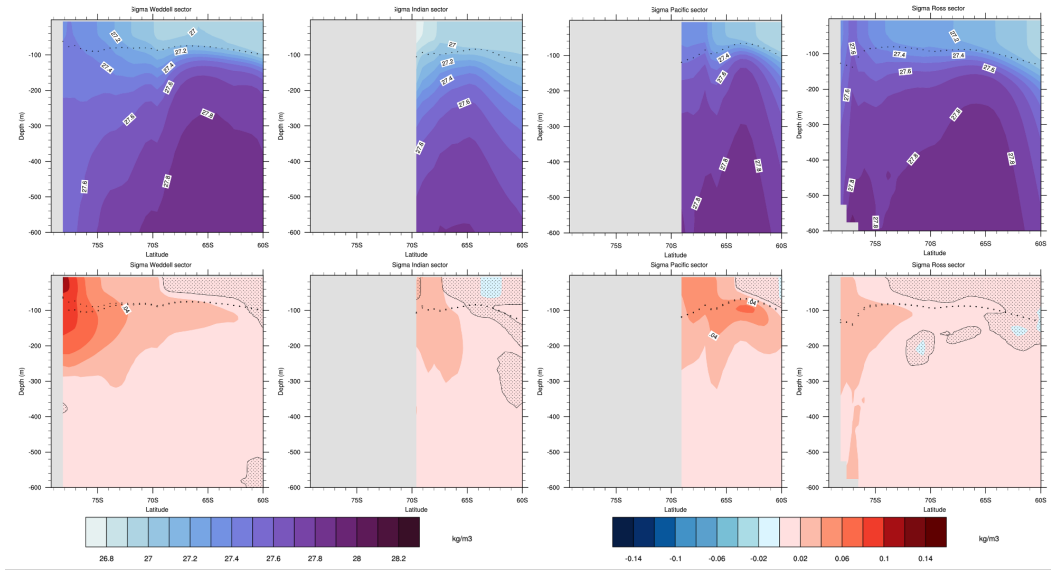


**Figure S6.** Winter (April-Sept) mean (top row) and difference (bottom row) transects for sigma ( $\text{kg m}^{-3}$ ) averaged over the Weddell sector (left column), Indian Ocean sector (second column), Pacific Ocean sector (third column), and Ross Sea sector (right column). All differences show MUSHY-BL99 and regions that are significantly different at the 95% confidence level do not have stippling.

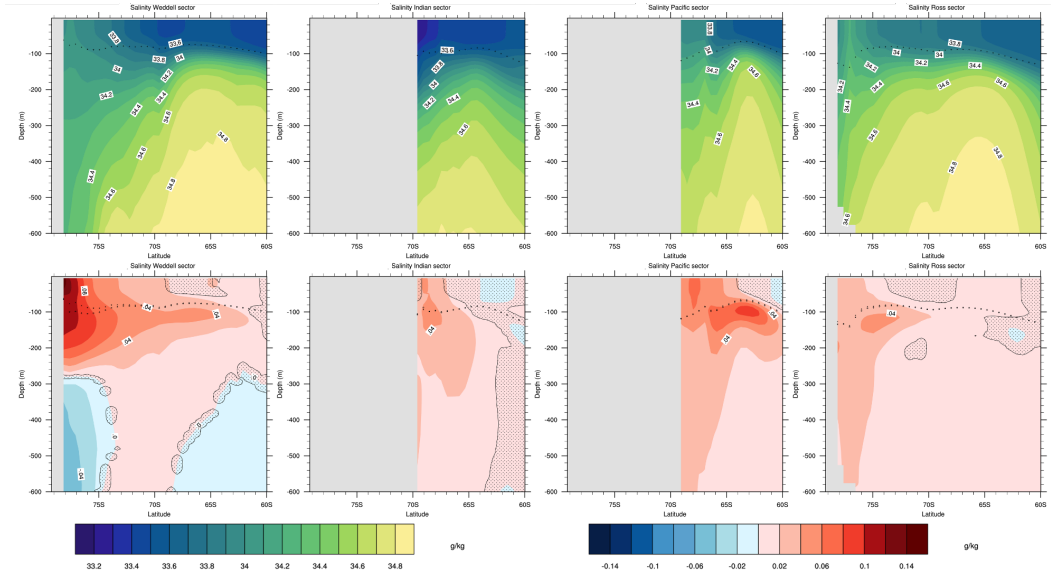


**Figure S7.** Winter (April-Sept) mean (top row) and difference (bottom row) transects for salinity ( $\text{g kg}^{-1}$ ) averaged over the Weddell sector (left column), Indian Ocean sector (second column), Pacific Ocean sector (third column), and Ross Sea sector (right column). All differences show MUSHY-BL99 and regions that are significantly different at the 95% confidence level do not have stippling.

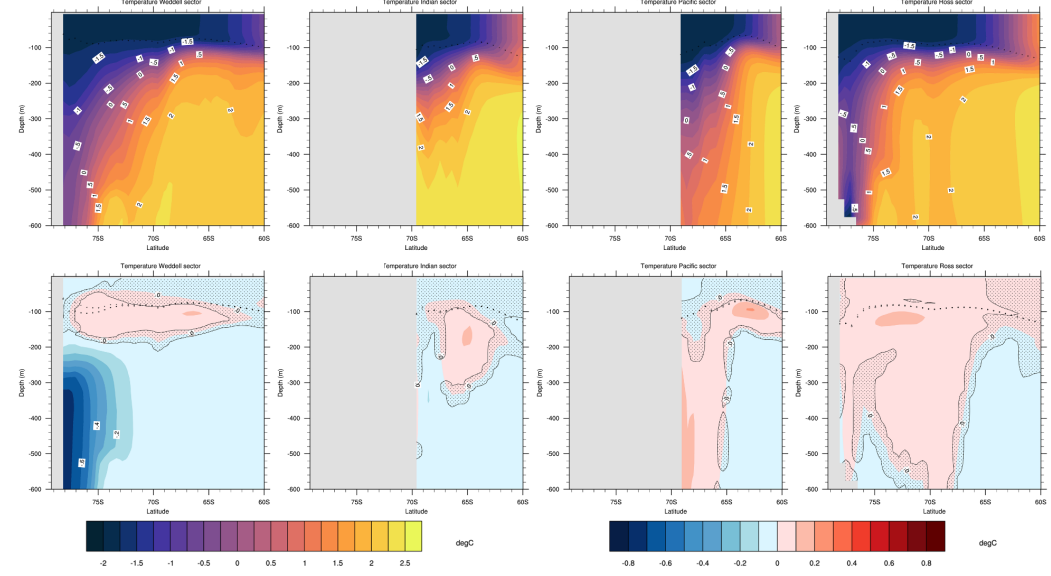


**Figure S8.** Winter (April-Sept) mean (top row) and difference (bottom row) transects for temperature ( $^{\circ}\text{C}$ ) averaged over the Weddell sector (left column), Indian Ocean sector (second column), Pacific Ocean sector (third column), and Ross Sea sector (right column). All differences show MUSHY-BL99 and regions that are significantly different at the 95% confidence level do not have stippling.

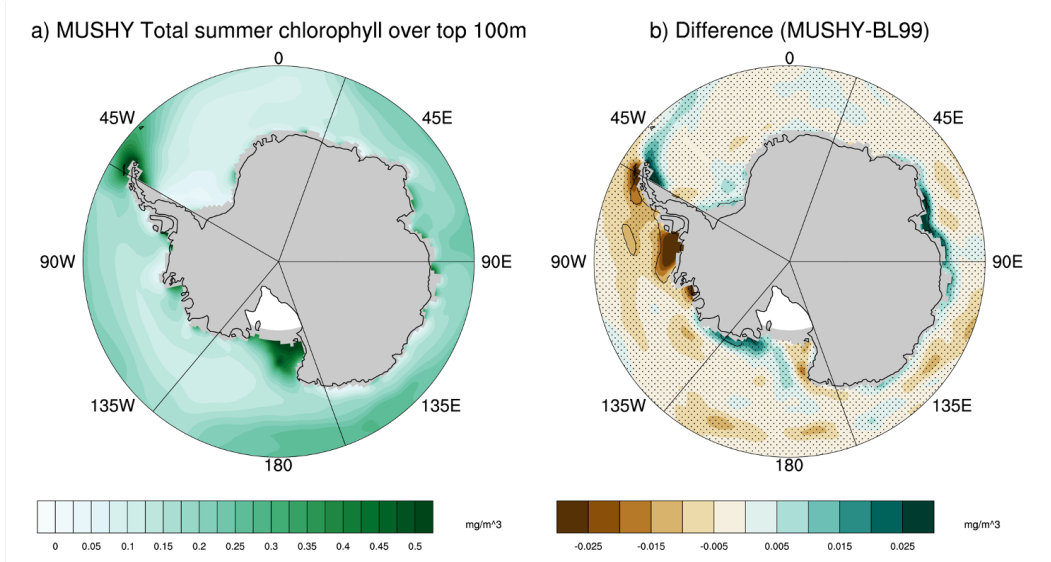


**Figure S9.** Summer (Oct-Mar) chlorophyll ( $\text{mg m}^{-3}$ ) integrated over the top 100m for a) MUSHY mean and b) difference (MUSHY-BL99). For difference plot regions that are significantly different at the 95% confidence level do not have stippling.

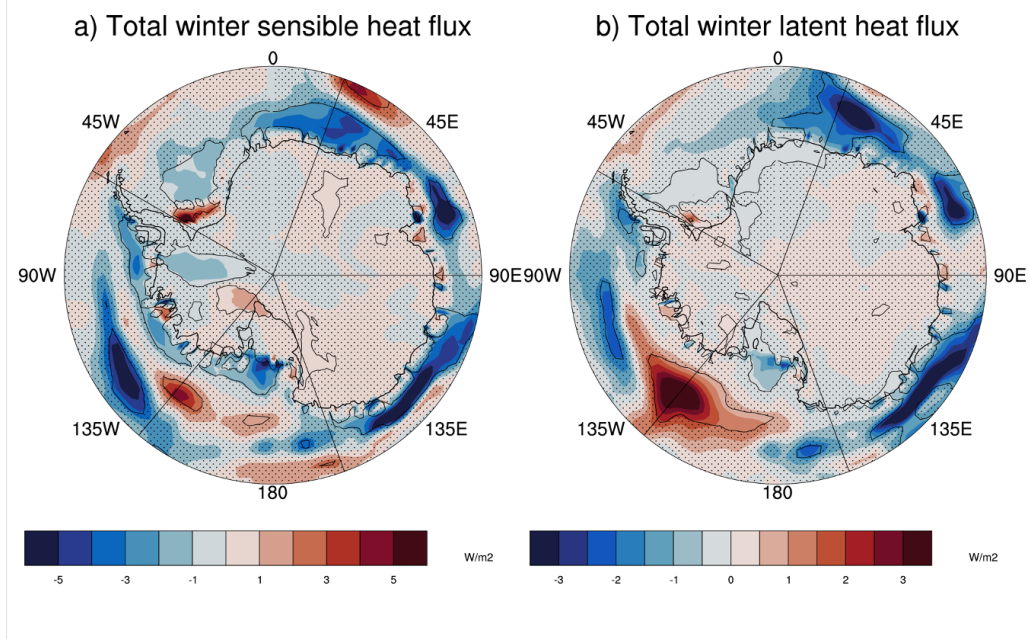


**Figure S10.** Winter (Apr-Sept) mean difference of a) sensible heat flux and b) latent heat flux ( $\text{W m}^{-2}$ ). Differences are MUSHY-BL99 and regions that are significantly different at the 95% confidence level do not have stippling.

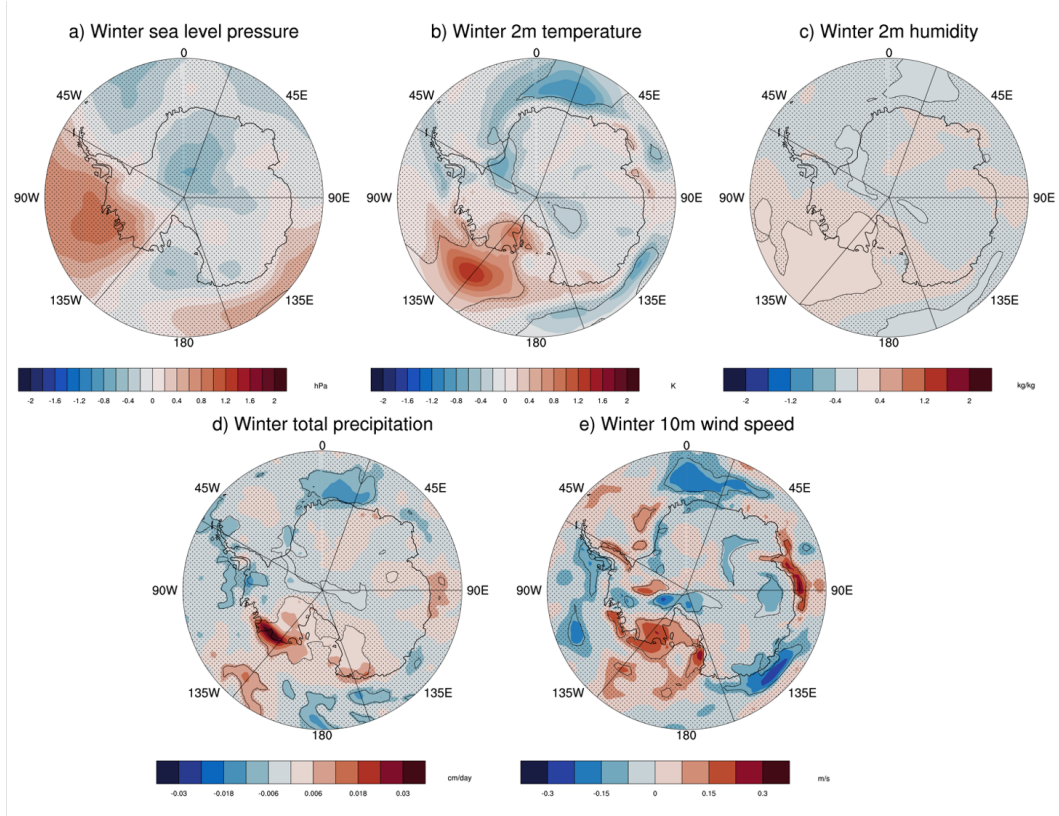


**Figure S11.** Winter (Apr-Sept) mean difference of a) sea level pressure (hPa), b) 2m Temperature (°C), c) 2m humidity (g kg<sup>-1</sup>), d) precipitation (cm day<sup>-1</sup>), e) 10m wind speed (m sec<sup>-1</sup>). Differences are MUSHY-BL99 and regions that are significantly different at the 95% confidence level do not have stippling.